

Modulation of the Mitochondrial Cytochrome bc₁ Complex Activity by Chromanols and Related Compounds

Andrea Müllebnner,[†] Anjan Patel,[‡] Werner Stamberg,[†] Katrin Staniek,[†] Thomas Rosenau,[‡] Thomas Netscher,[§] and Lars Gille^{*†}

Molecular Pharmacology and Toxicology Unit, Department of Biomedical Sciences, University of Veterinary Medicine Vienna, Veterinärplatz 1, A-1210 Vienna, Austria, Department of Chemistry, University of Natural Resources and Applied Life Sciences, Muthgasse 18, A-1190 Vienna, Austria, and Research and Development, DSM Nutritional Products, P.O. Box 2676, CH-4002 Basel, Switzerland

Received September 15, 2009

Tocopherols (α -, β -, γ -, and δ -Toc) and tocopheryl quinones (α -, β -, γ -, and δ -TQ) were recently suggested to modulate mitochondrial electron transfer in mammals. Intriguingly, Tocs and stigmatellin, a potent inhibitor of the mitochondrial cytochrome (cyt) bc₁ complex, possess a common structural feature: the chroman core. Therefore, we studied the interference of Tocs as well as synthetic model compounds (low molecular weight TQ analogues and tetramethyl chromanones) at the mitochondrial cyt bc₁ complex. Enzymatic experiments revealed that besides the inhibitor stigmatellin, among natural vitamin E-related derivatives, γ -TQ/ δ -TQ and, among synthetic compounds, TMC2O (6-hydroxy-4,4,7,8-tetramethyl-chroman-2-one) were most effective in decreasing the cyt bc₁ activities. Stopped-flow photometric and low-temperature electron paramagnetic resonance spectroscopic experiments showed for TMC2O an inhibition of electron transfer to cyt c₁ and a modulation of the environment of the Rieske iron–sulfur protein (ISP). Docking experiments suggest a binding interaction of the 6-OH group and 1-O atom/2-C(=O) group of TMC2O with Glu-271 (cyt b) and His-161 (ISP) in the cyt bc₁ complex, respectively. This binding pose is similar but not identical to the potent inhibitor stigmatellin. The data suggest that chroman-2-ones are possible templates for modulatory molecules for the cyt bc₁ target.

Introduction

The biological functions of vitamin E-related compounds have been of interest in biomedical research for several decades (1, 2). When the importance of oxygen radicals in the pathogenesis of various diseases was recognized, substances to combat oxidative stress became of potential therapeutic interest (3, 4). The observation that a major function of the vitamin E family (among others, see ref 5) is the scavenging of lipophilic reactive oxygen species boosted the application of these compounds as food supplements and for adjuvant therapy (6–8). The functions of vitamin E and its metabolites are far from being clear today, in spite of the long research history (9, 10).

Among the compounds of the vitamin E group, α -tocopherol (α -Toc)¹ was recognized as the most important and abundant lipid radical scavenger in mammalian tissues, while additional effects of the non- α -homologues (Tocs not permethylated at

the aromatic core), among them γ -Toc, were attributed to the scavenging of reactive nitrogen species and other electrophiles (11). A toxicological reason for the observed preference of α -Toc vs γ -Toc in mammalian tissues could be the metabolism of incompletely aryl-methylated Tocs to arylating γ -tocopheryl quinones (γ -TQ) vs the nonaryllating α -TQ (12). This is in line with findings that quinone metabolites of γ - and δ -Tocs possess cytostatic properties against cancer cells, while the corresponding α -metabolites are ineffective in this respect (13). In addition, several other functions of individual vitamin E compounds, such as regulation of gene expression and signal transduction, were recognized (5). In spite of the overwhelming number of scientific publications about α -Toc and partially also γ -Toc, the knowledge about the bioactivity of degradation products of Toc, such as TQ, epoxides, and various addition products to lipids (10, 14) arising in the mammalian organism, is scarce, especially with respect to their toxicological and pharmacological effects.

Tocs chemically belong to the class of chromans. In some applications, it has been shown that the chroman structure is similarly important to pharmacological effects as is the phenolic OH group. For example, troglitazone, an oral antidiabetic drug, contains a chromanol moiety, although radical scavenging is not its primary mode of action (15, 16). This suggests that the pattern of polar/apolar interaction sites in chromans/chromanols provides templates for specific enzyme/receptor binding sites. In this context, the question arises whether Toc derivatives interact with electron transport enzymes in the inner mitochondrial membrane, such as the cytochrome (cyt) bc₁ complex. Possible targets at this complex could be overall electron transfer (respiration), superoxide formation, proton pumping, and other functions. In any case, a binding of Toc-related compounds

* To whom correspondence should be addressed. Tel: +43-1-25077-4407. Fax: +43-1-25077-4490. E-mail: Lars.Gille@vetmeduni.ac.at.

[†] University of Veterinary Medicine Vienna.

[‡] University of Natural Resources and Applied Life Sciences.

[§] DSM Nutritional Products.

¹ Abbreviations: Asc, ascorbate; ATQ, atovaquone; cyt, cytochrome; DMSO, dimethyl sulfoxide; dUQH₂, decylubiquinol; IC₅₀, concentration at which 50% inhibition occurs; ISP, iron–sulfur protein; MOPS, 3-morpholino-1-propane sulfonic acid; Myx, myxothiazole; P_{ow}, octanol/water partition coefficient; QSAR, quantitative structure–activity relationship; Stig, stigmatellin {2-[(7E,9E,11E)-4,6-dimethoxy-3,5,11-trimethyl-trideca-7,9,11-trienyl]-8-hydroxy-5,7-dimethoxy-3-methyl-chromen-4-one}; TMC2O, 6-hydroxy-4,4,7,8-tetramethyl-chroman-2-one; TMC4O, 6-hydroxy-2,2,7,8-tetramethyl-chroman-4-one; Toc, tocopherol (all congeners); TQ, tocopheryl quinone (all congeners); α -TQ₀, 2-(3-hydroxy-3-methyl-butyl)-3,5,6-trimethyl-1,4-benzoquinone (TQ having the 4,8,12-trimethyldecyl side chain replaced by a methyl group); γ -TQ₀, 5-(3-hydroxy-3-methyl-butyl)-2,3-dimethyl-1,4-benzoquinone; UQ, ubiquinone; UQH₂, ubiquinol.

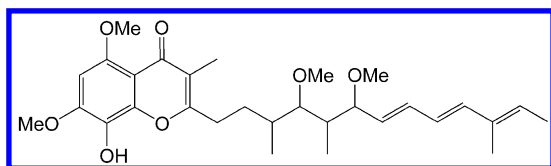


Figure 1. Structure of the mitochondrial inhibitor Stig.

would be a prerequisite to modulatory functions. Recently, Cuddihy and co-workers (17) reported the stimulation of mitochondrial superoxide release by increasing concentrations of α -Toc in mitochondria and observed higher respiratory control values at higher α -Toc concentrations. They suggested a modulatory activity of the chromanol α -Toc and the *para*-benzoquinone α -TQ through binding to the cyt bc_1 complex. Therefore, the question arose to which extent Toc-related molecules bind to the cyt bc_1 complex and which structures are responsible for binding. According to crystal structures of the cyt bc_1 complex, the entrance channels to these ubiquinone (UQ) (Q_i pocket)/ubiquinol (UQH₂) (Q_o pocket) binding sites are located in the lipid membrane and favor binding of molecules with lipophilic properties, such as UQ and Toc compounds. While the Q_o site is located close to the outer face of the inner mitochondrial membrane, Q_i has a position close to the inner face of this membrane. In this context, it is noteworthy that stigmatellin (Stig, Figure 1), a potent inhibitor of the cyt bc_1 complex, has a chromene (unsaturated chroman) core and resembles structural elements of chromanols. For α -TQ, a *para*-quinone metabolite of Toc, an interaction with several redox enzymes natively binding endogenous UQs was reported, leading partially to its reduction to the corresponding hydroquinone (α -TQH₂) (18). Besides the toxicological questions, the inhibition of the mitochondrial cyt bc_1 complex in species other than mammals is of general pharmacological interest. For these reasons, we studied the extent and mechanism of inhibitory effects of natural (α -, β -, γ -, and δ -Toc and α -, β -, γ -, and δ -TQ) and synthetic (low molecular weight TQ analogues and chromanones) compounds.

Materials and Methods

Chemicals. All-*rac*- α -Toc, sucrose, NaCl, NaH₂PO₄, NaN₃, FeCl₃, EDTA, glycerol, ascorbic acid, KH₂PO₄, dimethyl sulfoxide (DMSO), and sodium dithionite were purchased from Merck. Cytochrome c, decylubiquinone, 3-morpholino-1-propane sulfonic acid (MOPS), RRR- β / δ -Tocs, and Triton X-100 were obtained from Sigma. All-*rac*- γ -Toc was from Calbiochem. KCN and Stig were obtained from Fluka. The TQs (α -, β -, γ -, and δ -TQ) were synthesized by oxidation of the corresponding Toc with FeCl₃ and subsequent chromatographic purification, by analogy to the method reported in ref 19. The low molecular weight analogues 2-(3-hydroxy-3-methyl-butyl)-3,5,6-trimethyl-[1,4]-benzoquinone (α -TQ₀) and 5-(3-hydroxy-3-methyl-butyl)-2,3-dimethyl-[1,4]-benzoquinone (γ -TQ₀) were prepared according to the same method using a modified chromatographic workup as described in ref 20. 6-Hydroxy-4,4,7,8-tetramethyl-chroman-2-one (TMC2O) and 6-hydroxy-2,2,7,8-tetramethyl-chroman-4-one (TMC4O) were synthesized according to ref 21. Decylubiquinol (dUQH₂) was prepared from decylubiquinone according to ref 19.

Preparation of the Mitochondrial Cyt bc_1 Complex. A beef heart mitochondrial suspension was prepared from fresh beef heart by differential centrifugation according to Smith (22). The preparation method of the cyt bc_1 complex was adopted from Schagger et al. (23). Briefly, after a centrifugation of the mitochondrial suspension at 27000g for 15 min, the pellet was resuspended in MOPS buffer (20 mM, pH 7.2) to give a protein concentration of 35 mg/mL. Mitochondria were partially solubilized by adding Triton X-100 (1.75%) and NaCl (600 mM), giving a protein concentration

of 26 mg/mL. The pellet obtained by ultracentrifugation at 100000g for 45 min was resuspended in a buffer containing 300 mM sucrose and 20 mM MOPS (pH 7.2), giving a protein concentration of 35 mg/mL. The resulting suspension was mixed with an equal volume of extraction buffer (4% Triton X-100, 1.2 M NaCl, 20 mM MOPS, 300 mM sucrose, and 2 mM NaN₃, pH 7.2) and stirred for 5 min. The supernatant obtained by ultracentrifugation (45 min, 100000g) was mixed with an equal volume of hydroxyapatite [prepared according to Tiselius et al. (24)] equilibrated with 0.5% Triton X-100, 250 mM NaCl, and 80 mM NaH₂PO₄ to bind cyt bc_1 complex. After a slow speed centrifugation (1 min, 430g), the bc_1 /hydroxyapatite sediment was washed with 5 volumes of buffer (0.05% Triton X-100, 250 mM NaCl, 110 mM NaH₂PO₄, and 2 mM NaN₃, pH 7.2). The washed sediment was filled into a preparative column, and the cyt bc_1 complex was eluted with buffer (0.25% Triton X-100, 0.2 M KH₂PO₄, and 2 mM NaN₃, pH 7.2). The crude detergent-solubilized cyt bc_1 complex was concentrated to 15 mg protein/mL by pressure filtration using Amicon YM100 membranes (Millipore). Finally, the enzyme preparation was purified by gel chromatography using a Sepharose CL-6B column eluted with 0.05% Triton X-100, 100 mM NaCl, 20 mM MOPS, and 2 mM NaN₃, pH 7.2. Freshly prepared cyt bc_1 contained up to 6.5 nmol cyt bc_1 complex/mg protein and was stored at 77 K after the addition of 25% glycerol.

Determination of Michaelis–Menten Parameters and Inhibition of the Quinol:cyt c^{3+} Oxidoreductase Activity. The activities of the respective compounds at the isolated cyt bc_1 complex were measured using 1.3 μ g/mL (6 nM) bovine heart cyt bc_1 complex protein. The enzyme was suspended in 1 mL of buffer (pH 7.2, 25 °C) containing 250 mM sucrose, 50 mM KH₂PO₄, 0.2 mM EDTA, 2.5 mM KCN, 2 mM NaN₃, and 100 μ M cyt c^{3+} . Then, the reaction mixture was incubated for 10 min at 25 °C with the required concentrations of test compounds dissolved in DMSO, never exceeding a total amount of 10 μ L of vehicle. Respective control experiments to obtain the noninhibited activity (100% activity) were performed in the presence of the corresponding amounts DMSO. Then, the reduction of cyt c^{3+} was measured photometrically as the difference of the absorbance at 550 nm (cyt c^{2+}) minus the absorbance at 540 nm (isosbestic point) after the addition of 75 μ M dUQH₂ over a time of 3 min using a Shimadzu Multispec 1501 diode array photometer. Experiments were carried out in the presence of KCN and NaN₃. The obtained slopes were corrected for the chemical reduction of cyt c^{3+} by dUQH₂ obtained in the absence of cyt bc_1 complex. The experiments in the absence of chroman compounds were carried out using 0–60 μ M dUQH₂ to obtain rate–substrate data for the determination of K_m and v_{max} . The enzymatic reduction rates were calculated using an extinction coefficient of $\epsilon_{550-540nm} = 19 \text{ mM}^{-1} \text{ cm}^{-1}$ for cyt c (25). All measurements were done in triplicate for each compound and dUQH₂ concentration.

Log Octanol/Water Partition Coefficient (P_{OW}) Calculation. Structures of all compounds were built and geometry optimized using Hyperchem 7.5 (26). Subsequently, the log P_{OW} was calculated using the quantitative structure–activity relationship (QSAR) properties module, which uses an algorithm of Viswanadhan et al. (27).

Inhibition of Cyt b and Cyt c_1 Presteady-State Reduction. Fast reduction kinetics of cytochromes in isolated cyt bc_1 complex were followed with an AMINCO DW2000 spectrometer equipped with a stopped-flow reactor (MilliFlow SLM). The two syringes of the reactor contained 2 mL of buffer (100 mM NaCl, 10 mM MOPS, and 0.05% Triton X-100, pH 6.0), 2 mM KCN, and 2 mM NaN₃. In addition, the two syringes contained either cyt bc_1 complex (4.8 μ M) or dUQH₂ (127 μ M), respectively. From both syringes, each 100 μ L was mixed per shot, and data acquisition was performed for 3 s following the absorbance difference at 564 (cyt b) and 577 nm (isosbestic point) for cyt b and the absorbance difference at 554 (cyt c_1) minus 540 nm (isosbestic point) for cyt c_1 using a fast filter mode. Control experiments were performed in the absence of dUQH₂. For inhibition experiments, TMC2O (500 μ M) and Stig (100 μ M) were admixed to the solution containing

the cyt *bc*₁ complex in one syringe at least 1 min prior to an experiment. Therefore, final concentrations after mixing in the optical cell of the stopped-flow unit were the half of the initial concentrations for inhibitors, cyt *bc*₁ and dUQH₂. For each sample, five kinetic traces were averaged by a computer program of own design. Cytochrome reduction rates were calculated by an exponential fitting function during the first second prior to reaching a steady-state absorbance. The performance of the stopped-flow system was tested mixing a solution of bromophenol blue with buffer and following the absorbance increase at the wavelength 592 nm using the absorbance at 650 nm as a reference. From the detectable portion of the absorbance increase, a maximal first order rate constant of 40 s⁻¹ was calculated. For the kinetics of cyt redox state, only rates below this limit were considered as reaction rates arising from cyt reduction. Spectra in the visible region of the presteady-state reduction were recorded by a Shimadzu Multispec MS1501 diode array photometer setting the resolution to 2 nm and the scan rate to 0.2 s. For this experiment, isolated *bc*₁ complex (3 μM) was diluted in 1 mL of buffer containing 100 mM NaCl, 10 mM MOPS, 0.05% Triton X-100, pH 6.0, 1 mM KCN, and 1 mM NaN₃ in a stirring cuvette. After preincubation (1 min) with vehicle (DMSO, control experiment), 250 μM TMC2O or 50 μM Stig data acquisition was started for a total of 30 s. Cyt *bc*₁ reduction was started by the addition of dUQH₂ (100 μM) at about 3 s, and total reduction was achieved by the addition of dithionite at 15 s. For evaluation of the data, spectra indicating the admixing of dUQH₂ were identified and considered as initial state (0 s), and consecutive spectra were selected for analysis of the cyt *b/cyt c*₁ reduction ratio.

EPR Spectroscopy of the Rieske Iron–Sulfur Center. Samples of oxidized Rieske iron–sulfur center (FeS) were prepared by suspending isolated bovine heart cyt *bc*₁ complex (63 μM) in 100 μL of buffer (250 mM sucrose, 50 mM KH₂PO₄, and 0.2 mM EDTA, pH 7.2) containing 10 mM NaN₃ and 2% (v/v) DMSO (vehicle for inhibitors). This reaction mixture was incubated for 20 min in quartz tubes (4 mm o.d.) and was then frozen in liquid nitrogen. Reduced Rieske iron–sulfur centers were prepared analogously but in the presence of 10 mM ascorbate (Asc) alone or additionally 500 μM TMC2O or 100 μM Stig (dissolved in DMSO). Low temperature EPR spectra were recorded using a Bruker EMX instrument equipped with a TE₁₀₂ cavity and a cryostat (Oxford ESR 900) cooled by liquid helium. Prior to the experiments, the cryostat and the helium transfer line were evacuated below 10⁻⁵ mbar by a turbo molecular pump (Pfeiffer TSH 064). The sample temperature was adjusted to 20 K by a temperature controller (Oxford ITC 503), a pump (Oxford GF3) for helium circulation, and a gas flow controller (Oxford VC 41). For EPR measurements, used were the following instrument settings: 9.47055 GHz microwave frequency, 10 mW microwave power, 3600 G center field, 1000 G sweep, 10 G modulation amplitude, 5.02 × 10⁵ receiver gain, 715 G/min scan rate, 0.163 s time constant, and 1 scan. The subtraction of spectra from reduced minus oxidized samples, baseline correction, and measurements of *g*-factors were performed using the software WINEPR (Bruker).

Molecular Modeling. The crystal structure 2A06 (28) of a bovine cyt *bc*₁ complex was chosen as a template for the study. In this structure, two UQ and two Stig molecules were bound into the two Q_i and two Q_o binding pockets, respectively. Because of the fact that Stig bound in the cyt *b* subunit of one monomer interacts with the Rieske FeS center of the other monomer, we extracted the C (cyt *b*) and the R (FeS) chain from the complex. Likewise, Stig bound between these two chains was extracted and later taken as reference for the initial position of the docked ligands. The Stig molecule from the crystal structure was edited by correcting bond order and adding hydrogens without disturbing its global structure and position. All other structures were built in Hyperchem (26) and subsequently optimized using the MM+ force field and finally stored as PDB files. Using Autodock Tools (29), molecular torsions of ligands were compiled into PDBQT files for Autodock 4.0 (30–32), and parameter files were created. The protein subunits were treated likewise, and in addition, charges of heme iron atoms were corrected manually. All dockings were performed using

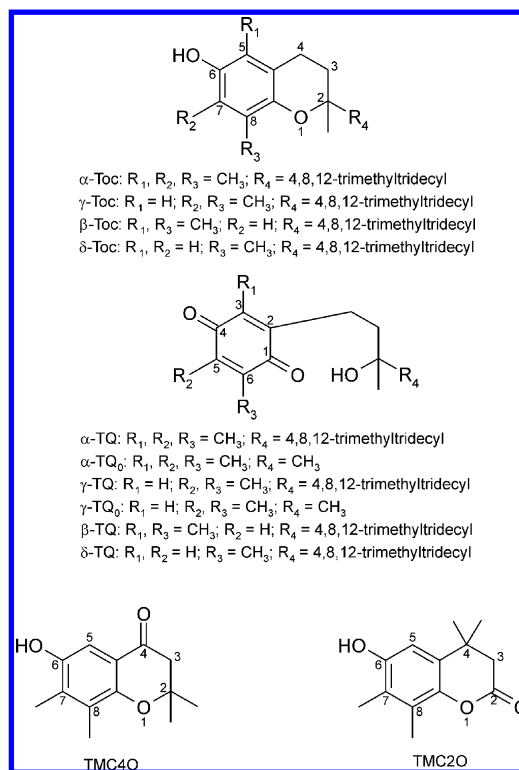


Figure 2. Structures of Toc derivatives and related compounds tested for their inhibiting properties in the isolated cyt *bc*₁ complex.

standard parameters except that 5 × 10⁶ energy evaluations and 100 docking runs were used. Analysis of docking results and preparation of figures was done by the Autodock Tools package.

Data Analysis. Mean values, SDs, and SEs of experimental data were calculated using Origin 6.1 (MicroCal). The concentrations at 50% inhibition (absolute IC₅₀ values) for experiments with cyt *bc*₁ complex were obtained from a nonlinear regression of the activity data [Origin 6.1 (MicroCal), custom function] according to a four parameter logistic model (4PL, Hill–Slope model) following the recommendations of the National Institute of Health. The absolute IC₅₀ was calculated according to eq 1 setting *v*_{bot} to 0% and *v*_{top} to 100% remaining activity. With the latter parameters fixed, slope and IC₅₀ were calculated from *v* (actual inhibition in %) as a function of inhibitor concentration (*c*_{inh}).

$$v = v_{\text{top}} + \frac{(v_{\text{top}} - v_{\text{bot}})}{1 + (c_{\text{inh}}/\text{IC}_{50})^{\text{slope}}} \quad (1)$$

Determination of Michaelis–Menten parameters *K*_m and *v*_{max} was performed by nonlinear regression [Origin 6.1 (MicroCal), custom function] of turnover number (*v*) as a function of the substrate concentration (*c*_{sub}) according to eq 2.

$$v = \frac{v_{\text{max}} \times c_{\text{sub}}}{K_{\text{m}} + c_{\text{sub}}} \quad (2)$$

Results

The compounds selected for this study belong to the group of Tocs (α -, β -, γ -, and δ -Toc) and their oxidation products, TQs (α -, β -, γ -, and δ -TQ). In addition to these compounds, naturally occurring as (*R,R,R*)-isomers, synthetic short-chain homologues of TQ (α -TQ₀ and γ -TQ₀) and the chromanones TMC2O and TMC4O were investigated. In the compounds tested (Stig, Figure 1, and Toc, chromanones, Figure 2), the chroman core is a common structural element. To assess inhibiting properties of Toc-related compounds (α -, β -, γ -,

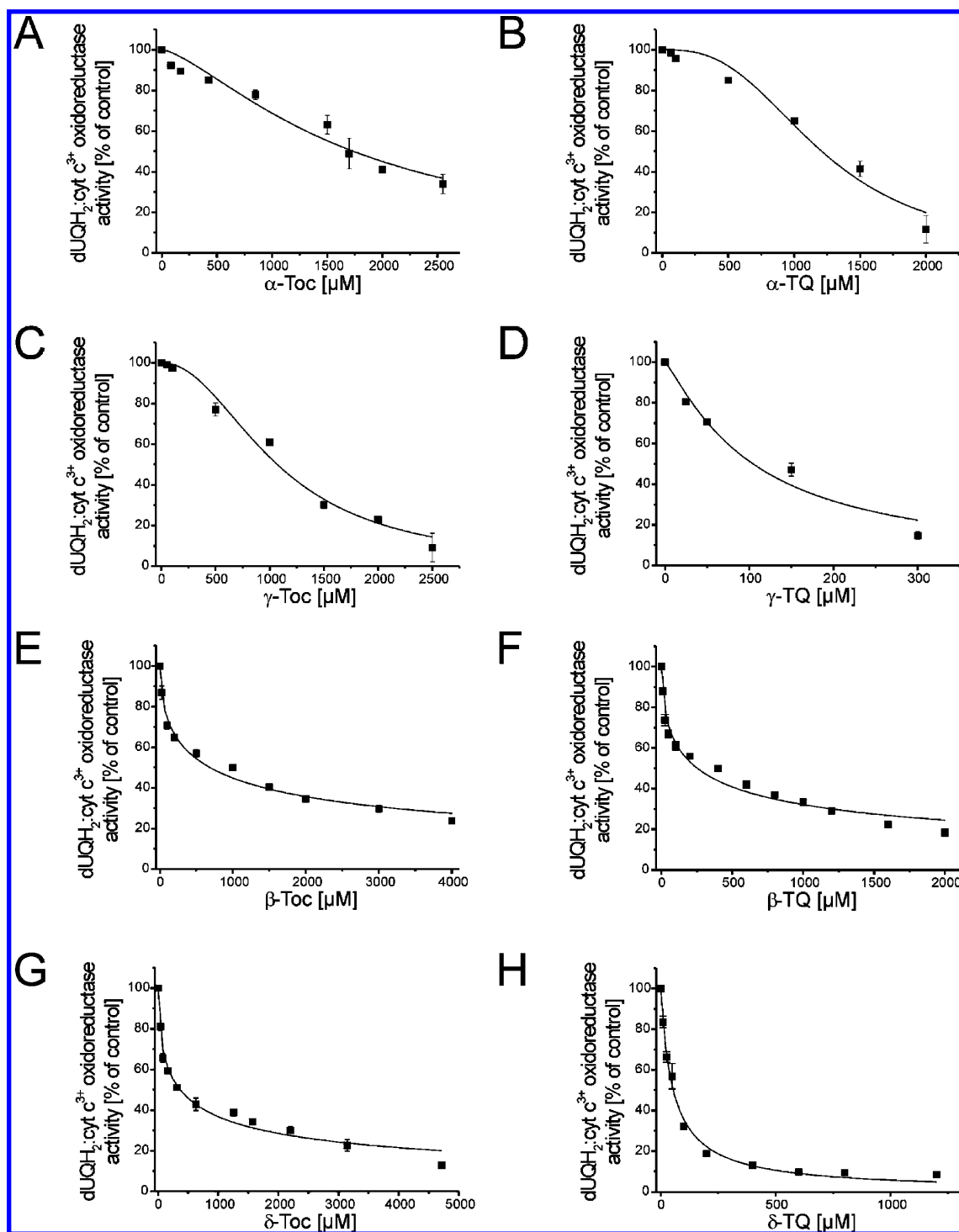


Figure 3. Decrease of $\text{dUQH}_2\text{:cyt } c^{3+}$ oxidoreductase activity of isolated $\text{cyt } bc_1$ complex in the presence of α -Toc (A), α -TQ (B), γ -Toc (C), γ -TQ (D), β -Toc (E), β -TQ (F), δ -Toc (G), and δ -TQ (H). The activity without inhibitor was set to 100%, and the subsequent inhibition was expressed in % of total activity. Each data point represents the mean \pm SE of three measurements. The assay was performed with three independent enzyme preparations. Data points were fitted by a four parameter logistic model (4PL, Hill–Slope model, eq 1) for the calculation of the IC_{50} values.

and δ -Toc; α -, β -, γ -, and δ -TQ; α - and γ -TQ₀; TMC2O; and TMC4O), the isolated $\text{cyt } bc_1$ complex from bovine heart was preincubated with the respective derivatives, and then, the remaining $\text{dUQH}_2\text{:cyt } c^{3+}$ oxidoreductase activity at a fixed dUQH_2 (75 μM) and fixed $\text{cyt } c^{3+}$ (100 μM) concentration was determined (Figure 3A–H for Toc and TQ congeners and Figure 4A–D for TQ₀ and TMC0 derivatives). In addition, the potent mitochondrial inhibitor Stig was studied in these experiments (Figure 4E). Control experiments were carried out in the presence of vehicle (DMSO) and served as reference values (100%). The activity in the

presence of Toc-related compounds was expressed in percent remaining activity of the control experiment (vehicle only). The maximum concentration of Toc-related compounds used was limited by the turbidity of assay solutions and was not further increased if about 80% inhibition (20% residual activity) was achieved (Figures 3 and 4). Therefore, it was not possible to verify whether 100% inhibition can be obtained in all cases. However, to compare the inhibition potency between the tested compounds, the concentrations at which 50% residual activity was obtained (absolute IC_{50}) were calculated (Table 1). These data demonstrate a moderate

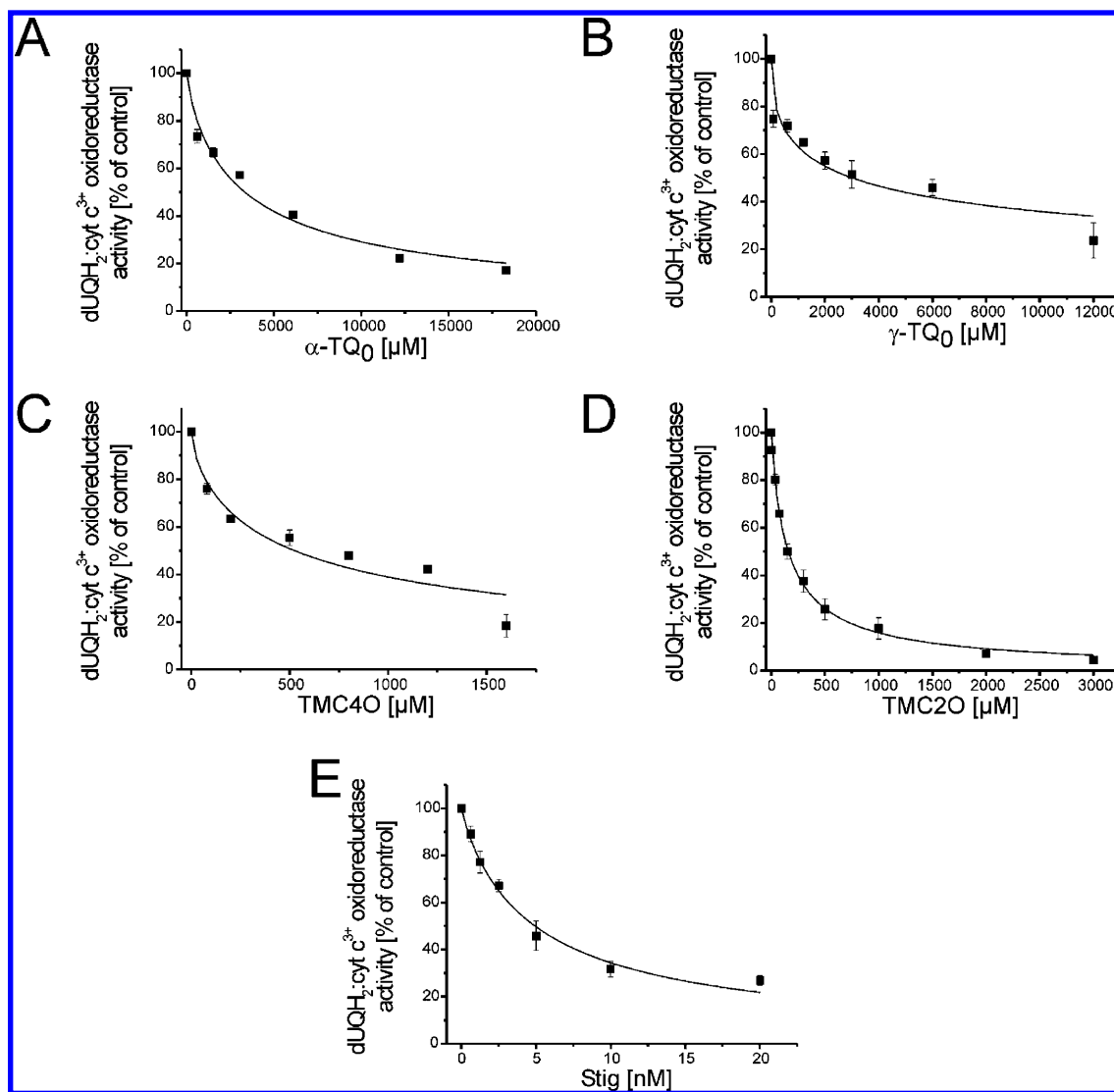


Figure 4. Decrease of dUQH₂:cyt c³⁺ oxidoreductase activity of isolated cyt *bc*₁ complex in the presence of α -TQ₀ (A), γ -TQ₀ (B), TMC40 (C), TMC20 (D), and Stig (E). The same conditions as in Figure 3 were used.

Table 1. Inhibition of the dUQH₂:cyt c³⁺ Oxidoreductase Activity by Toc and Related Compounds^a

compound	IC ₅₀ (μ M)	log $P_{OW,calcd}$
α -Toc	1739 \pm 127	9.6
γ -Toc	1069 \pm 62	9.13
β -Toc	686 \pm 56	9.13
δ -Toc	367 \pm 40	8.67
α -TQ	1209 \pm 71	8.58
γ -TQ	104 \pm 8	8.31
β -TQ	252 \pm 24	8.31
δ -TQ	53 \pm 4	8.03
α -TQ ₀	3331 \pm 194	2.76
γ -TQ ₀	3017 \pm 719	2.49
TMC40	524 \pm 70	2.13
TMC20	159 \pm 10	3.15
Stig	0.0049 \pm 0.0004	4.01

^a Results were obtained using 75 μ M dUQH₂, 100 μ M cyt c³⁺, and 6 nM isolated cyt *bc*₁ complex. The partition coefficient (log $P_{OW,calcd}$) of all compounds was calculated using the QSAR module of Hyperchem.

inhibition by γ - and δ -TQ and TMC20, while other Toc-/TQ-related compounds were less effective.

To elucidate the mechanism of inhibition, the most effective low molecular weight compound TMC20 was selected for further studies. In a first step, the catalytic properties of the cyt *bc*₁ complex in the presence of vehicle only (Figure 5, 0 μ M TMC20) were characterized by measuring the turnover rates

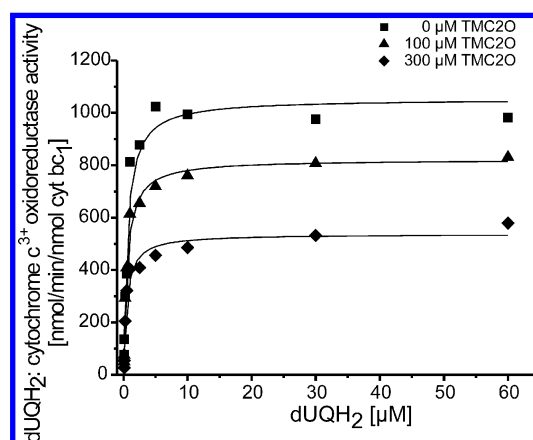


Figure 5. dUQH₂:cyt c³⁺ oxidoreductase activity of isolated bovine heart cyt *bc*₁ complex and its inhibition by TMC20. Variation of the dUQH₂:cyt c³⁺ oxidoreductase activity with increasing dUQH₂ concentrations in the absence and in the presence of 100 μ M and 300 μ M TMC20. Data points were fitted by a nonlinear model of the Michaelis–Menten equation (eq 2) for determination of K_m and v_{max} .

for dUQH₂:cyt c³⁺ oxidoreductase activity with increasing concentrations of dUQH₂. Fitting activity data to the Michaelis–Menten equation by nonlinear regression maximal turnover rates

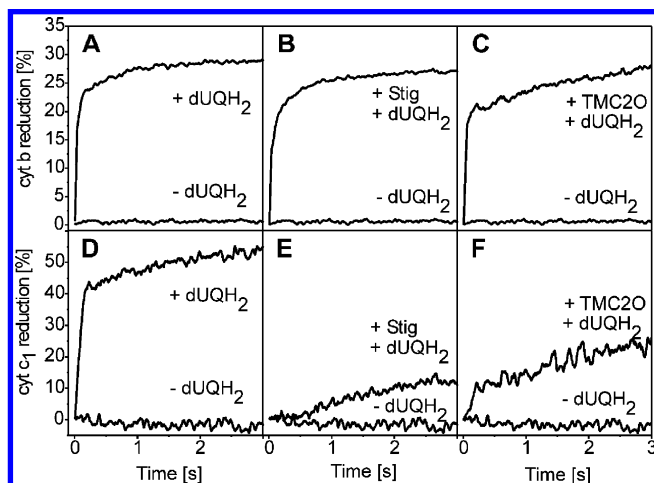


Figure 6. Reduction of cytochromes b (A–C) and c₁ (D–F) of isolated bovine heart cyt bc₁ complex (2.4 μM) by dUQH₂ (63.5 μM) in the absence (A and D) and presence of the inhibitors Stig (50 μM, B and E) and TMC2O (250 μM, C and F) measured in a stopped-flow unit. Each panel shows the absorbance trace with (+dUQH₂) and without (–dUQH₂) substrate. The reduction states of b and c₁ cytochromes were detected by the absorbance difference at 564 nm minus the absorbance at 577 nm and the absorbance difference at 554 nm minus the absorbance at 540 nm, respectively, and normalized on the total amount of cyt reduced by dithionite.

of $v_{\max} = 1053 \pm 46$ nmol/min/nmol cyt bc₁ and a Michaelis–Menten constant of $K_m = 0.58 \pm 0.12$ μM dUQH₂ were obtained. To assess the inhibition type of TMC2O, analogous measurements were done in the presence of 100 and 300 μM concentrations of this compound (Figure 5). Calculation of v_{\max} for 100 and 300 μM TMC2O resulted in 821 ± 28 and 536 ± 28 nmol/min/nmol cyt bc₁, respectively. Assessment of K_m for 100 and 300 μM TMC2O gave 0.53 ± 0.08 and 0.48 ± 0.10 μM dUQH₂, respectively. Accordingly, the ratios v_{\max}/K_m (given in nmol/min/nmol cyt bc₁/μM) for 0, 100, and 300 μM TMC2O were 1791, 1526, and 1099, respectively. Therefore, the decrease of v_{\max} , the decrease of the ratio v_{\max}/K_m , and the almost unchanged K_m with increasing concentrations of TMC2O suggest a noncompetitive inhibition type.

The question whether TMC2O binds to the Q_o pocket of the cyt bc₁ complex was studied by stopped-flow photometry on a subsecond time scale (Figure 6). In this experiment, the reduction of b and c₁ cytochromes by dUQH₂ was detected as the difference of the absorbance at 564 nm minus the absorbance at 577 nm and as the difference of the absorbance at 554 nm minus the absorbance at 540 nm, respectively. Because of different effects of inhibitors on the turbidity during the rapid mixing, absorbance data of stopped-flow experiments were normalized to the dithionite reducible amount of the respective cytochromes within the individual experiment (100%). Noninhibited reduction of cytochromes in the experiments achieved first order rate constants of 40 ± 7 s⁻¹ for cyt b and 15 ± 3 s⁻¹ for cyt c₁ (Figure 6A,D). The rate constant for cyt b reduction was already in the range of the detection limit of our stopped-flow system around 40 s⁻¹. In the presence of Stig, a drastically decreased cyt c₁ reduction at a rate of 1.3 ± 0.3 s⁻¹ and a slightly slower rate of cyt b reduction (17 ± 4 s⁻¹) was observed (Figure 6B,E). These data confirmed the preferred binding of Stig at the Q_o pocket of the cyt bc₁ complex. The compound TMC2O did not strongly influence the cyt b reduction rate [26 ± 11 s⁻¹ (Figure 6C)] but suppressed cyt c₁ reduction (0.4 ± 0.1 s⁻¹, Figure 6F). Dual wavelength stopped-flow experiments provide accurate information on kinetic reaction parameters since first order rate constants do not depend on the amplitude of

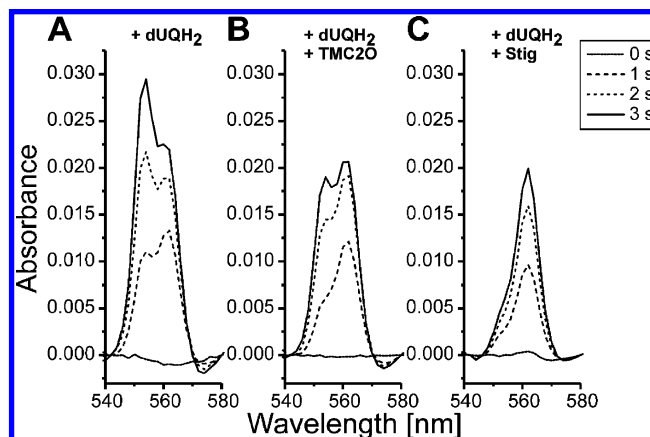


Figure 7. Visible spectra of isolated cyt bc₁ complex (3 μM) during the reduction by 100 μM dUQH₂ in the absence of any inhibitor (A), in the presence of 250 μM TMC2O (B), and in the presence of 50 μM Stig (C) using a diode array photometer. Turbidity changes during the reaction were corrected by subtracting a linear baseline adjusting the absorbance at 540 and 578 nm to zero for each scan. After consecutive scans were started in 0.2 s intervals, the reaction was initiated by adding dUQH₂. The scan at which the addition became visible by baseline shift was set as the initial (0 s) spectrum, and three other spectra at 1, 2, and 3 s were displayed.

absorbance changes. However, to verify the influence of turbidity changes on the amount of cyt reduction states after 3 s multiwavelength scans of the cyt bc₁ reduction followed by baseline correction for turbidity changes in the absence and presence of inhibitors after manual admixing of dUQH₂ were performed. After baseline correction, the spectra shown in Figure 7 were obtained. In the absence of inhibitors, both rapid cyt b (right peak) and cyt c₁ (left peak) reduction were observed (Figure 7A). The reduction of cyt c₁ is delayed in the presence of TMC2O (Figure 7B) and almost abolished if Stig (Figure 7C) was present. The amounts of cyt b reduction ($A_{564\text{nm}} - A_{578\text{nm}}$) after 3 s were 27, 28, and 28% of the dithionite reducible portion for the control, TMC2O, and Stig, respectively. The reduction states of cyt c₁ ($A_{554\text{nm}} - A_{540\text{nm}}$) after the same time were 53, 34, and 10% of the dithionite reducible portion for the control, TMC2O, and Stig, respectively. These data suggested a minor influence of TMC2O and Stig on the cyt b redox state, while Stig strongly and TMC2O moderately decreased the extent of cyt c₁ reduction within this time scale.

To further characterize TMC2O binding to the cyt bc₁ complex, we studied the influence of this molecule on the coordination of the Rieske iron–sulfur protein (ISP) in comparison with Stig. EPR signals of the Rieske FeS cluster from isolated cyt bc₁ complex were observed at 20 K (Figure 8). Oxidized cyt bc₁ complex gave no characteristic EPR signal under these conditions. The baseline obtained from the oxidized complex was subtracted from the subsequent recordings of reduced cyt bc₁ complex. Upon incubation of the complex with Asc, the characteristic anisotropic signal of the Rieske FeS center became visible (Figure 8A) giving peaks at $g_x = 2.0288$, $g_y = 1.8958$, and $g_z = 1.767$ (Table 2). Repeating this experiment after preincubation with Stig, a shift of the absorption lines g_x by -0.0041 , g_y by -0.009 , and g_z by $+0.02$ was observed (Figure 8C). For the chromanone compound TMC2O in the corresponding experiment, shifts of g_x by -0.0064 , g_y by $+0.0001$, and g_z by $+0.03$ were observed (Figure 8B). The observed spectral changes in each case suggested a binding of the respective molecules to the cyt bc₁ complex influencing the Rieske FeS cluster.

To visualize possible interacting amino acid residues for TMC2O within the bovine cyt bc₁ protein, the binding of this

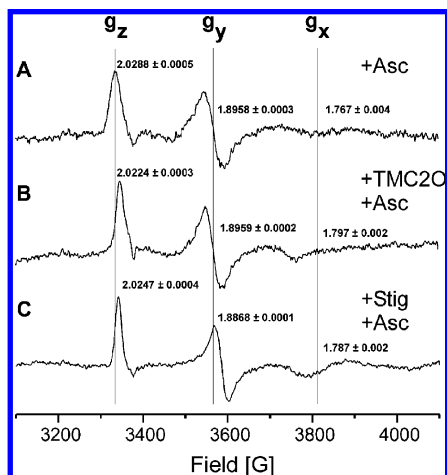


Figure 8. EPR spectrum of the Rieske iron–sulfur center of isolated bovine heart cyt *bc*₁ complex and the influence of inhibitors. Low temperature EPR spectra at 20 K were obtained from 37.8 μ M cyt *bc*₁ complex, 10 mM Asc, and 10 mM NaN₃ in buffer (250 mM sucrose, 50 mM potassium phosphate, and 0.2 mM EDTA, pH 7.2). For all samples, the spectra were obtained by subtraction of the spectrum of Asc-reduced cyt *bc*₁ complex minus a spectrum of the oxidized sample. The reduced samples contained (A) Asc only, (B) Asc plus 500 μ M TMC2O, and (C) Asc plus 100 μ M Stig. *g*-Factors represent means \pm standard deviations of two independent cyt *bc*₁ samples and triplicate EPR recordings.

Table 2. Shifts of the *g*-Factors *g*_z, *g*_y, and *g*_x of the Rieske ISP of the Cyt *bc*₁ Complex and the Influence of Inhibitors Measured in This and Other Studies^a

study	cyt <i>bc</i> ₁ complex	<i>g</i> _z	<i>g</i> _y	<i>g</i> _x
Ding et al. (52)	native reduced	2.026	1.893	1.765
	+ Stig	0.0000	−0.0050	+0.0210
	+ Myx	+0.0080	+0.0010	+0.0050
Kessl et al. (53)	native reduced	2.028	1.899	1.75
	+ Stig	−0.0020	−0.0110	+0.0300
	+ ATQ	+0.0060	−0.0110	+0.0100
this work	native reduced	2.0288	1.8958	1.767
	+ Stig	−0.0041	−0.0090	+0.0200
	+ TMC2O	−0.0064	+0.0001	+0.0300

^a For calculation of the shifts induced by inhibitors, the respective native reduced cyt *bc*₁ complex of the study was always used.

molecule to the Q_o pocket was analyzed by docking experiments using the program Autodock (30–32). For this purpose, the crystal structure 2A06 of dimeric bovine heart cyt *bc*₁ complex deposited by Berry et al. (28) containing UQ-6 (UQ₆) and Stig was used. The Q_o binding pocket formed by cyt *b* subunit of one monomer and the Rieske FeS cluster of the other monomer were extracted, and a box for the ligand of 19 × 19 × 24 Å³ was placed around the binding pocket. Likewise, bound Stig was extracted from the crystal structure and edited to obtain a molecule with proper bond orders and appropriate hydrogen substitutions. Ligand molecules were optimized by the MM+ force fields, and docking was performed using Autodock's Lamarckian algorithm. Structures with the lowest binding energies were extracted from the log files and graphically arranged using Autodock Tools (29). The position of the ligand molecule (TMC2O, Figure 9B) and interacting amino acid residues (ISP side with His-161; cyt *b* side with Glu-271) obtained by docking experiments in comparison with the redocked position of Stig (Figure 9A) in the crystal structure were obtained.

Discussion

In mitochondria, Toc (mostly α -Toc) coexists with UQ and the α -Toc oxidation product α -TQ (33). In addition, the presence

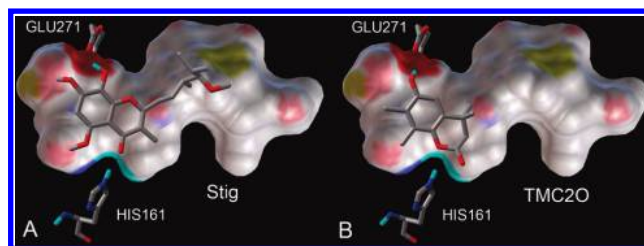


Figure 9. Results of docking experiments to the Q_o pocket of the crystal structure 2A06 of dimeric cyt *bc*₁ complex from bovine heart for Stig (A) and TMC2O (B). The pictures show the orientation of the molecules within the binding pocket formed by cyt *b* (Glu-271) and the Rieske iron–sulfur (His-161) subunit for the lowest energy conformation of each molecule. The surface of the ligand molecule is colored by atom type showing oxygen and polar hydrogen atoms in red and blue, respectively. A part of the side chain of Stig is not visible due to the front clipping plane.

of epoxy-hydroperoxy-tocopherones and epoxy-TQs in mitochondria after artificially induced lipid peroxidation has been demonstrated (34). In the inner mitochondrial membrane of rat liver mitochondria, the ratio of UQ: α -Toc: α -TQ is about 100:10:0.5 (33). Therefore, the question arose whether Toc or TQ derivatives in the inner mitochondrial membrane might have functions beyond radical scavenging, such as interference in UQ functions.

A few reports on the modulation of the cyt *bc*₁ function by nonsubstrate molecules have been published in the past, describing functional changes by well-known inhibitors (35, 36), phospholipids (37, 38), nutritionally relevant compounds, such as erucic acid and cholesterol (39), and vitamin E-related compounds (17). Recently, Cuddihy and co-workers demonstrated that restoration of α -Toc and α -TQ modulates the release of superoxide radicals from the cyt *bc*₁ complex in brain mitochondria from vitamin E-deficient rats (17). They proposed a binding of α -Toc and α -TQ to the Q_o pocket, which interfere with the electron transfer at this site.

Because of the detectability of some of the tested compounds in mammalian cells (α -Toc, α -TQ, γ -Toc, and γ -TQ), it is evident that none of these structures inhibits the cyt *bc*₁ complex as strongly as the potent inhibitor Stig does (Figure 4E and Table 1). Nevertheless, Stig and Toc/chromanone compounds share some structural features (Figures 1 and 2). Therefore, the question arose as to which structures in the tested compounds favor a Stig-like inhibition (at the Q_o site) of the cyt *bc*₁ complex.

In mitochondrial membranes, the potency of an inhibitor is influenced by its affinity to the respective enzyme and its actual concentration inside the membrane, which can be very different from the bulk phase concentration. A usual parameter to approximate the concentration ratio between the aqueous phase and the lipid phase is the log *P*_{ow} coefficient (Table 1). In contrast, in the detergent-solubilized *bc*₁ complex, the enzyme is homogeneously dispersed in the aqueous phase, and no strong enrichment of lipophilic compounds is expected. The membrane concentration of native UQ-10 was approximated around 5–10 mM (40, 41).

In a previous study (33), we observed α -Toc concentrations of up to 0.19 nmol/mg protein in mitoplasts from rat liver mitochondria. Because the protein distribution in the matrix and inner membrane of rat liver mitochondria is 68 and 22% (42), the content of α -Toc in the inner membrane is about 0.76 nmol/mg protein. Assuming that 1 mg of protein in the inner mitochondrial membrane corresponds to 1 μ L of lipid (41), the α -Toc concentration is about 0.76 mM. Therefore, the IC₅₀ for α -Toc of about 1.7 mM (Table 1 and Figure 3A) is only about twice as high as the physiological concentration. We thus

expected that the physiological concentration of α -Toc has an influence on dUQH₂:cyt *c*³⁺ oxidoreductase activity of the cyt *bc*₁ complex.

γ -Toc, a minor component in mitochondrial membranes under physiological conditions, exhibited IC₅₀ values (Table 1 and Figure 3C) about half that of α -Toc. Other Toc congeners (β - and δ -Toc) possess even lower IC₅₀ values (Table 1 and Figure 3E,G). It has been shown that α -TQ and α -TQ₀ can serve as alternative substrates for the Q_i site of the mitochondrial cyt *bc*₁ complex (18, 33). On the other hand, α -TQH₂ and α -TQ₀H₂ are very poor substrates for the Q_o site of this complex (18, 33). This limited suitability as a substrate suggested that their presence could retard UQ-mediated electron transfer at the cyt *bc*₁ complex. Although α -TQ exhibits a slightly lower IC₅₀ than α -Toc, this may not suggest α -TQ as a strong inhibitor *in vivo* since its concentration is 20–50 times lower than that of α -Toc. This, however, does not exclude that α -TQH₂ might act as inhibitor or that α -TQ/ α -TQH₂ might modulate the formation of reactive oxygen species at the cyt *bc*₁ complex as suggested for rhodoquinol (43). The comparison of short chain analogues (α -TQ₀ and γ -TQ₀, Table 1 and Figure 4A,B) to their lipophilic counterparts (α -TQ and γ -TQ, Table 1 and Figure 3B,D) indicated that lipophilic structures partially enhance the inhibition strength. While for α -TQ vs α -TQ₀ the inhibition increase is small, γ -TQ is several magnitudes more effective than γ -TQ₀; an effect that cannot be explained only by different lipophilicity. Docking studies for γ -TQ₀ (data not shown) revealed that among favorable binding poses, both orientations with the chromanol 6-OH (“head on”) toward His-161/Glu-271 and reverse orientations (6-OH oriented to the channel entrance) are possible. Therefore, the additional lipophilic side chain in γ -TQ vs γ -TQ₀ would favor the head on orientation, which could be a possible explanation for the efficiency of γ -TQ for cyt *bc*₁ inhibition at the Q_o site. In addition, a decreasing degree of methyl substitution increases inhibition by Toc and TQ compounds. This might be an alternative explanation as to why α -Toc is retarded in the organism in comparison with its congeners.

Furthermore, the question arises whether γ -TQ due to its Michael acceptor properties can attach to protein thiol groups in the cyt *bc*₁ complex. While the incubation time in the cyt *bc*₁ activity assay used in this study was too short to explore this effect, Wong and Liebler (44) have shown that in cells incubated over 24 h, a cyt *c*₁ precursor, which is required for cyt *bc*₁ function, is labeled by an *N*-ethylmaleimido derivative, mimicking electrophilic quinones, such as γ -TQ.

Although these considerations focus on the binding of these molecules to the Q_o site, an interaction of TQ and Toc derivatives with the Q_i site of the cyt *bc*₁ complex might also be involved in the observed effects. For example, the reduction of TQ to TQH₂ is preferably expected at the Q_i site of the cyt *bc*₁ complex (18). However, this does not necessarily mean that inhibition by TQ can only occur at the Q_i site, since in many cases inhibiting molecules are not substrates of the respective targets.

On the basis of the results of steady-state kinetic experiments, which suggest that a methyl substitution at the chromane core decreases inhibition (IC₅₀: α -Toc > γ -Toc > β -Toc > δ -Toc) (Figure 3 and Table 1), chromanone compounds (TMC2O and TMC4O) were synthesized to explore whether chromanone structures (Figures 2 and 4C,D and Table 1) further enhance binding to the Q_o pocket of the cyt *bc*₁ complex. Among Toc-related compounds, TMC2O was suitable for further mechanistic studies since (i) it was among the most effective inhibiting compounds in the steady-state experiments (Figure 4D and Table

1); (ii) it is moderately lipophilic and not prone to micelle formation (40) as the strongly lipophilic Toc and TQ, allowing effective binding to the isolated cyt *bc*₁ complex; and (iii) chromanone structures were reported to possess bactericidal properties and are, therefore, of general pharmacological interest (45–48).

To assess the type of inhibition, the cyt *bc*₁ complex activity was studied at different TMC2O and dUQH₂ concentrations (Figure 5). The decreasing *v*_{max} and the unchanged *K*_m with increasing TMC2O concentrations suggest a noncompetitive inhibition. This is in contrast to Stig, which was shown to bind competitively with UQ and UQH₂ to the cyt *bc*₁ complex (36). Therefore, TMC2O is less efficient than Stig and exhibits a slightly different binding behavior.

Presteady-state kinetic measurements (Figure 6) in the stopped-flow system were technically limited to maximum rates of about 40 s⁻¹. The wavelength pairs chosen for monitoring the reduction of cyt *b* by dUQH₂ about equally report cyt *b*_L (absorbance maximum at 562 nm) and cyt *b*_H (absorbance maximum at 566 nm), taking into account the slit width of 2 nm. For cyt *b* reduction in the absence of inhibitors, the rates (40 s⁻¹) already achieved the technical limit of the stopped-flow unit. However, actual cyt *b* reduction rates triggered by dUQH₂ are expected to be considerably higher as assessed from other kinetic experiments [\sim 90 s⁻¹, yeast cyt *bc*₁, 50 μ M menaquinol, conventional stopped-flow (49); 270 s⁻¹, bovine heart cyt *bc*₁, photoreleasable dUQH₂ (50)]. During this rapid phase, less than half of the dithionite-reducible cyt *b* was reduced. The rapid phase in the noninhibited complex was followed by a further slow reduction phase with a rate of 1.59 \pm 0.07 s⁻¹. In general, cyt *c*₁ reduction rates were reported to be slower [e.g., \sim 4 s⁻¹, yeast cyt *bc*₁, 50 μ M menaquinol, conventional stopped-flow (49); 60 s⁻¹, bovine heart cyt *bc*₁, photoreleasable dUQH₂ (50)] than cyt *b* reduction rates. This was also the case in our experiments, which gave a reduction rate for cyt *c*₁ of about 15 s⁻¹. Therefore, observed experimental rates depend on kinetic techniques, origin of cyt *bc*₁ complex, artificial substrate, buffer composition, and substrate concentration. Rates observed in our experiments for the cyt *b* reduction represent only a lower limit and are within the expected range for cyt *c*₁ reduction. In spite of these limitations, the stopped-flow system was sufficiently sensitive to qualitatively characterize the influence of inhibitors and TMC2O on the cyt *bc*₁ reduction by dUQH₂. In the presence of Stig, the cyt *b* reduction rate (17 \pm 4 s⁻¹) was only slightly slower than in the noninhibited complex (Figure 6). In contrast, cyt *c*₁ reduction rate decreased to 1.3 \pm 0.3 s⁻¹, which is qualitatively in line with findings of Snyder and Trumpower (51) for menaquinol and Stig. TMC2O required a higher concentration than Stig to influence cyt reduction. TMC2O at 250 μ M efficiently delayed cyt *c*₁ reduction. Spectra in the visible region obtained during cyt *bc*₁ reduction suggest that both Stig and TMC2O have only a minor influence on the final cyt *b* redox state (Figure 7).

The Rieske ISP of the cyt *bc*₁ complex exhibits in the reduced state a characteristic EPR signal at low temperatures (<30 K) at *g*-factors around 2.0, 1.9, and 1.8 and is influenced by inhibitors. For Stig, myxothiazole (Myx), and atovaquone (ATQ), the order of sensitivity was *g*_x \gg *g*_y > *g*_z \approx 0, *g*_z > *g*_x > *g*_y \approx 0, and *g*_y > *g*_x > *g*_z, respectively (52, 53) (Table 2, first two sections). This suggests that the *g*_x absorption line around 1.8 is most sensitive toward the presence of some inhibitors (but not all). It has been proposed that the shift of the *g*_x band

and to a lesser extent of other bands as seen in the presence of Stig (Figure 8C) is related to the H-bond strength between the His-161 of the ISP and the inhibitor molecule or UQH₂ in the cyt *bc*₁ complex (54). Because of analysis of crystal structures, Glu-272 (Glu-271 in 2A06) as another interacting residue for H-bond formation with substrate and inhibitors was proposed (54). Our experiment reproduced the inhibitor influence by the observation of shifts of the g_x to higher and g_z bands to lower g -factors upon addition of Stig (Figure 8C vs A). In view of the fact that Stig is a highly potent inhibitor, it was surprising that although higher concentrations of TMC2O were required, the latter compound did produce a spectral shift of the EPR lines of the FeS in the ISP (Figure 8B). For TMC2O, the sensitivity order of g -factors was $g_x \gg g_z > g_y \approx 0$ (Table 2). This suggests that TMC2O, although with lower affinity, interacts with the ISP but possesses binding sites in the Q_o pocket similar but not identical to Stig.

By docking experiments, we intended to explore the effects of the molecular similarity of Toc-derived compounds and Stig. A structure of the cyt *b* subunit with a bound ISP from the crystal structure 2A06 (28) was used as a receptor in our docking experiments. The program in the rigid protein docking mode reproduced the position of Stig in the crystal structure 2A06 (28) within a root-mean-square deviation (rmsd) from reference structure of 0.832 Å and the interaction of the chroman core of Stig with Glu-271 and His-161 (Figure 9A).

For chroman-6-ols, docking experiments predicted conformations among the docking poses with the lowest energy, which orient the 6-OH group toward Glu-271 and the 1-O toward the His-161 residue. The lower steric shielding of 6-OH in β -, γ -, and δ -Toc by the lack of methyl groups in comparison with α -Toc might provide a rationale for their stronger binding (Table 1). Likewise, for TMC2O, the orientation of the 6-OH group toward Glu-271 was favored (Figure 9B). Nevertheless, these data do not exclude that binding of lipophilic TQ/Toc congeners to the Q_i site is also involved in their inhibition of the cyt *bc*₁ activity. While the qualitative results of docking experiments are plausible, the quantitative docking approximations (predicted inhibition constants, data not shown) were less favorable and could not reproduce the order of inhibition strength over all compounds.

Conclusions

The 6-hydroxy chroman structures of Toc-related and the *para*-benzoquinone structure of TQ-related molecules can modulate the function of the mitochondrial cyt *bc*₁ complex. For both Toc and TQ, an incomplete methyl substitution (β -, γ -, and δ -congeners) increases the inhibitory potential in comparison with fully substituted α -congeners. This affinity can be further enhanced by the introduction of keto groups into the chroman ring, thus leading to chromanones. For TMC2O, it was shown that it binds to the Q_o pocket of the cyt *bc*₁ complex and delays the electron transfer from dUQH₂ to cyt *c*₁ in the complex. This study demonstrated that the interaction of chromanols and chromanones with the cyt *bc*₁ complex is not an unspecific effect but is based on their pattern of polar vs apolar structural motifs.

Acknowledgment. The generous help of Dr. Massimiliano D'Arienzo (University of Milano), Dr. Michael Elser and Prof. Oliver Diwald (Technical University of Vienna) in setting up the helium cryostat for low temperature EPR measurements is gratefully acknowledged.

References

- Brigelius-Flohe, R., and Traber, M. G. (1999) Vitamin E: function and metabolism. *FASEB J.* 13, 1145–1155.
- Brigelius-Flohe, R. (2009) Vitamin E: The shrew waiting to be tamed. *Free Radical Biol. Med.* 46, 543–554.
- Burton, G. W., and Ingold, K. U. (1989) Vitamin E as an in vitro and in vivo antioxidant. *Ann. N. Y. Acad. Sci.* 570, 7–22.
- Pryor, W. A. (2000) Vitamin E and heart disease: Basic science to clinical intervention trials. *Free Radical Biol. Med.* 28, 141–164.
- Azzi, A., Gysin, R., Kempna, P., Munteanu, A., Villacorta, L., Visarius, T., and Zingg, J. M. (2004) Regulation of gene expression by alpha-tocopherol. *Biol. Chem.* 385, 585–591.
- Kline, K., Lawson, K. A., Yu, W., and Sanders, B. G. (2007) Vitamin E and cancer. *Vitam. Horm.* 76, 435–461.
- Singh, U., and Devaraj, S. (2007) Vitamin E: Inflammation and atherosclerosis. *Vitam. Horm.* 76, 519–549.
- Di Sario, A., Candelaresi, C., Omenetti, A., and Benedetti, A. (2007) Vitamin E in chronic liver diseases and liver fibrosis. *Vitam. Horm.* 76, 551–573.
- Zingg, J. M. (2007) Vitamin E: An overview of major research directions. *Mol. Aspects Med.* 28, 400–422.
- Gille, L., Rosenau, T., Kozlov, A. V., and Gregor, W. (2008) Ubiquinone and tocopherol: Dissimilar siblings. *Biochem. Pharmacol.* 76, 289–302.
- Hoglen, N. C., Waller, S. C., Sipes, I. G., and Liebler, D. C. (1997) Reactions of peroxynitrite with gamma-tocopherol. *Chem. Res. Toxicol.* 10, 401–407.
- Wang, X., Thomas, B., Sachdeva, R., Arterburn, L., Frye, L., Hatcher, P. G., Cornwell, D. G., and Ma, J. (2006) Mechanism of arylating quinone toxicity involving Michael adduct formation and induction of endoplasmic reticulum stress. *Proc. Natl. Acad. Sci. U.S.A.* 103, 3604–3609.
- Jones, K. H., Liu, J. J., Roehm, J. S., Eckel, J. J., Eckel, T. T., Stickrath, C. R., Triola, C. A., Jiang, Z., Bartoli, G. M., and Cornwell, D. G. (2002) Gamma-tocopherol quinone stimulates apoptosis in drug-sensitive and multidrug-resistant cancer cells. *Lipids* 37, 173–184.
- Yamauchi, R. (2007) Addition products of alpha-tocopherol with lipid-derived free radicals. *Vitam. Horm.* 76, 309–327.
- Fukunaga-Takenaka, R., Shirai, Y., Yagi, K., Adachi, N., Sakai, N., Merino, E., Merida, I., and Saito, N. (2005) Importance of chroman ring and tyrosine phosphorylation in the subtype-specific translocation and activation of diacylglycerol kinase alpha by D-alpha-tocopherol. *Genes Cells* 10, 311–319.
- Nagasaka, Y., Kaku, K., Nakamura, K., and Kaneko, T. (1995) The new oral hypoglycemic agent, CS-045, inhibits the lipid peroxidation of human plasma low density lipoprotein in vitro. *Biochem. Pharmacol.* 50, 1109–1111.
- Cuddihy, S. L., Ali, S. S., Musiek, E. S., Lucero, J., Kopp, S. J., Morrow, J. D., and Dugan, L. L. (2008) Prolonged alpha-tocopherol deficiency decreases oxidative stress and unmasks alpha-tocopherol-dependent regulation of mitochondrial function in the brain. *J. Biol. Chem.* 283, 6915–6924.
- Gille, L., Gregor, W., Staniek, K., and Nohl, H. (2004) Redox-interaction of alpha-tocopherol quinone with isolated mitochondrial cytochrome *bc*₁ complex. *Biochem. Pharmacol.* 68, 373–381.
- Gille, L., Staniek, K., and Nohl, H. (2001) Effects of tocopherol quinone on the heart: Model experiments with xanthine oxidase, heart mitochondria, and isolated perfused rat hearts. *Free Radical Biol. Med.* 30, 865–876.
- Patel, A., Netscher, T., Gille, L., Mereiter, K., and Rosenau, T. (2007) Novel tocopherol compounds XXV: synthesis and comparison of the para-quinones of all four homologous tocopherol model compounds and their 3,4-dehydro derivatives. *Tetrahedron* 63, 5312–5318.
- Yenes, S., and Messeguer, A. (1999) A study of the reaction of different phenol substrates with nitric oxide and peroxynitrite. *Tetrahedron* 55, 14111–14122.
- Smith, A. L. (1962) Preparation, properties, and conditions for assay of mitochondria: Slaughterhouse material, small scale. *Methods Enzymol.* 10, 81–86.
- Schägger, H., Link, T. A., Engel, W. D., and von Jagow, G. (1986) Isolation of the eleven protein subunits of the *bc*₁ complex from beef heart. *Methods Enzymol.* 126, 224–237.
- Tiselius, A., Hjerten, S., and Levin, Ö. (1956) Protein chromatography on calcium phosphate columns. *Arch. Biochem. Biophys.* 65, 132–155.
- Brandt, U., and Okun, J. G. (1997) Role of deprotonation events in ubihydroquinone:cytochrome *c* oxidoreductase from bovine heart and yeast mitochondria. *Biochemistry* 36, 11234–11240.
- Hypercube, Inc. (1994) Hyperchem Professional 7.51, Hypercube, Inc., Gainesville, FL.

- (27) Viswanadhan, V. N., Ghose, A. K., Revankar, G. R., and Robins, R. K. (1989) Atomic physicochemical parameters for 3 dimensional structure directed quantitative structure-activity relationships. 4. Additional parameters for hydrophobic and dispersive interactions and their application for an automated superposition of certain naturally-occurring nucleoside antibiotics. *J. Chem. Inf. Comput. Sci.* 29, 163-172.
- (28) Huang, L. S., Cobessi, D., Tung, E. Y., and Berry, E. A. (2005) Binding of the respiratory chain inhibitor antimycin to the mitochondrial bc₁ complex: A new crystal structure reveals an altered intramolecular hydrogen-bonding pattern. *J. Mol. Biol.* 351, 573-597.
- (29) Sanner, M. F. (1999) Python: A programming language for software integration and development. *J. Mol. Graphics Modell.* 17, 57-61.
- (30) Goodsell, D. S., and Olson, A. J. (1990) Automated docking of substrates to proteins by simulated annealing. *Proteins Struct., Funct., Gen.* 8, 195-202.
- (31) The Scripps Research Institute (2006) Autodock 4.0, The Scripps Research Institute, California.
- (32) Morris, G. M., Goodsell, D. S., Halliday, R. S., Huey, R., Hart, W. E., Belew, R. K., and Olson, A. J. (1998) Automated docking using a Lamarckian genetic algorithm and an empirical binding free energy function. *J. Comput. Chem.* 19, 1639-1662.
- (33) Gregor, W., Staniek, K., Nohl, H., and Gille, L. (2006) Distribution of tocopheryl quinone in mitochondrial membranes and interference with ubiquinone-mediated electron transfer. *Biochem. Pharmacol.* 71, 1589-1601.
- (34) Ham, A. J., and Liebler, D. C. (1995) Vitamin E oxidation in rat liver mitochondria. *Biochemistry* 34, 5754-5761.
- (35) von Jagow, G., and Link, T. A. (1986) Use of specific inhibitors on the mitochondrial bc₁ complex. *Methods Enzymol.* 126, 253-271.
- (36) Covian, R., Pardo, J. P., and Moreno-Sanchez, R. (2002) Tight binding of inhibitors to bovine bc₁ complex is independent of the Rieske protein redox state. Consequences for semiquinone stabilization in the quinol oxidation site. *J. Biol. Chem.* 277, 48449-48455.
- (37) Yu, C. A., and Yu, L. (1980) Structural role of phospholipids in ubiquinol-cytochrome c reductase. *Biochemistry* 19, 5715-5720.
- (38) Schägger, H., Hagen, T., Roth, B., Brandt, U., Link, T. A., and von Jagow, G. (1990) Phospholipid specificity of bovine heart bc₁ complex. *Eur. J. Biochem.* 190, 123-130.
- (39) Gille, L., and Nohl, H. (2001) The ubiquinol/bc₁ redox couple regulates mitochondrial oxygen radical formation. *Arch. Biochem. Biophys.* 388, 34-38.
- (40) Fato, R., Estornell, E., Di Bernardo, S., Pallotti, F., Parenti, C. G., and Lenaz, G. (1996) Steady-state kinetics of the reduction of coenzyme Q analogs by complex I (NADH:ubiquinone oxidoreductase) in bovine heart mitochondria and submitochondrial particles. *Biochemistry* 35, 2705-2716.
- (41) Estornell, E., Fato, R., Castelluccio, C., Cavazzoni, M., Parenti-Castelli, G., and Lenaz, G. (1992) Saturation kinetics of coenzyme Q in NADH and succinate oxidation in beef heart mitochondria. *FEBS Lett.* 311, 107-109.
- (42) Schnaitman, C., and Greenawalt, J. W. (1968) Enzymatic properties of the inner and outer membranes of rat liver mitochondria. *J. Cell Biol.* 38, 158-175.
- (43) Cape, J. L., Strahan, J. R., Lenaus, M. J., Yuknis, B. A., Le, T. T., Shepherd, J. N., Bowman, M. K., and Kramer, D. M. (2005) The respiratory substrate ridoquinol induces Q-cycle bypass reactions in the yeast cytochrome bc(1) complex: Mechanistic and physiological implications. *J. Biol. Chem.* 280, 34654-34660.
- (44) Wong, H. L., and Liebler, D. C. (2008) Mitochondrial protein targets of thiol-reactive electrophiles. *Chem. Res. Toxicol.* 21, 796-804.
- (45) Emami, S., Kebriaeezadeh, A., Zamani, M. J., and Shafiee, A. (2006) Azolychromans as a novel scaffold for anticonvulsant activity. *Bioorg. Med. Chem. Lett.* 16, 1803-1806.
- (46) Cottiglia, F., Dhanapal, B., Sticher, O., and Heilmann, J. (2004) New chromanone acids with antibacterial activity from *Calophyllum brasiliense*. *J. Nat. Prod.* 67, 537-541.
- (47) Xu, Z. Q., Buckheit, R. W., Stup, T. L., Flavin, M. T., Khilevich, A., Rizzo, J. D., Lin, L., and Zembower, D. E. (1998) In vitro anti-human immunodeficiency virus (HIV) activity of the chromanone derivative, 12-oxocalanolide A, a novel NNRTI. *Bioorg. Med. Chem. Lett.* 8, 2179-2184.
- (48) Yang, G., Jiang, X., and Yang, H. (2002) Development of novel pesticides based on phytoalexins: Part 2. Quantitative structure-activity relationships of 2-heteroaryl-4-chromanone derivatives. *Pest. Manage. Sci.* 58, 1063-1067.
- (49) Snyder, C. H., and Trumpower, B. L. (1999) Ubiquinone at center N is responsible for triphasic reduction of cytochrome b in the cytochrome bc₁ complex. *J. Biol. Chem.* 274, 31209-31216.
- (50) Hansen, K. C., Schultz, B. E., Wang, G., and Chan, S. I. (2000) Reaction of *Escherichia coli* cytochrome bo(3) and mitochondrial cytochrome bc(1) with a photoreleasable decylubiquinol. *Biochim. Biophys. Acta* 1456, 121-137.
- (51) Snyder, C., and Trumpower, B. L. (1998) Mechanism of ubiquinol oxidation by the cytochrome bc(1) complex: Pre-steady-state kinetics of cytochrome bc(1) complexes containing site-directed mutants of the Rieske iron-sulfur protein. *Biochim. Biophys. Acta* 1365, 125-134.
- (52) Ding, H., Robertson, D. E., Daldal, F., and Dutton, P. L. (1992) Cytochrome bc₁ complex [2Fe-2S] cluster and its interaction with ubiquinone and ubihydroquinone at the Q_o site: A double-occupancy Q_o site model. *Biochemistry* 31, 3144-3158.
- (53) Kessl, J. J., Lange, B. B., Merbitz-Zahradnik, T., Zwicker, K., Hill, P., Meunier, B., Palsdottir, H., Hunte, C., Meshnick, S., and Trumpower, B. L. (2003) Molecular basis for atovaquone binding to the cytochrome bc₁ complex. *J. Biol. Chem.* 278, 31312-31318.
- (54) Berry, E. A., and Huang, L. S. (2003) Observations concerning the quinol oxidation site of the cytochrome bc₁ complex. *FEBS Lett.* 555, 13-20.

TX900333F